A test-particle method for the calculation of the three-particle distribution function of the hard-sphere fluid: density functional theory and simulation

1999 J. Phys.: Condens. Matter 11 3789

(http://iopscience.iop.org/0953-8984/11/19/301)

J. Phys.: Condens. Matter **11** (1999) 3789–3798. Printed in the UK PII: S0953-8984(99)99717-5

A test-particle method for the calculation of the three-particle distribution function of the hard-sphere fluid: density functional theory and simulation

A González, F L Román and J A White

Departamento de Física Aplicada, Facultad de Ciencias, Universidad de Salamanca, 37008 Salamanca, Spain

Received 26 November 1998, in final form 15 February 1999

Abstract. The three-particle distribution function $g^{(3)}$ of the homogeneous hard-sphere fluid is studied by means of the test-particle method of Percus. We consider an inhomogeneous situation in which the position of two particles is fixed and the inhomogeneous density profile that arises is related to $g^{(3)}$. The profile is calculated via Monte Carlo (MC) simulation and density functional theory (DFT). The results of the simulation are compared with standard MC results for the homogeneous fluid in order to check the numerics. The results of DFT are compared with MC data, showing a significant improvement over the well-known superposition approximation of Kirkwood.

One of the main aspects of the equilibrium statistical mechanics of liquids and dense fluids is the study of the microscopic structure, since it provides valuable information on the thermodynamic properties of the system. It is well known that the equilibrium structure of a fluid can be described by means of the so-called n-particle densities $\rho^{(n)}(\boldsymbol{r}_1, \ldots, \boldsymbol{r}_n)$ where $\boldsymbol{r}_i$ denotes the coordinates of the particle i (see, e.g., reference [1] for a definition of $\rho^{(n)}$). Closely related to the n-particle densities are the n-particle distribution functions [1]:

$$g^{(n)}(\boldsymbol{r}_1, \ldots, \boldsymbol{r}_n) = \rho^{(n)}(\boldsymbol{r}_1, \ldots, \boldsymbol{r}_n) \Big/ \prod_{i=1}^{n} \rho^{(1)}(\boldsymbol{r}_i). \tag{1}$$

For a homogeneous system, $\rho^{(1)}(\boldsymbol{r}) = \rho_{\mathrm{B}}$ where ρ_{B} is the bulk density of the fluid, and thus ${\rho_{\mathrm{B}}}^n g^{(n)}(\boldsymbol{r}_1, \ldots, \boldsymbol{r}_n) = \rho^{(n)}(\boldsymbol{r}_1, \ldots, \boldsymbol{r}_n)$. In addition, if the system is isotropic, its two-particle distribution function $g^{(2)}(\boldsymbol{r}_1, \boldsymbol{r}_2)$ only depends on $r = |\boldsymbol{r}_1 - \boldsymbol{r}_2|$; in this case $g^{(2)}$ is written as $g(r)$ and called the radial distribution function (RDF) [1]. For hard spheres or Lennard-Jones fluids, excellent approximations for $g(r)$ are available in the literature [1]. However, much less is known about the three-particle distribution function. Similarly, the knowledge of the one-particle structure of inhomogeneous fluids has experienced an important advance in recent years [2], but only a few studies of its two-particle structure are available in the literature (see below). One of the reasons for the lack of information on these higher-order distribution functions is the fact that the three-particle functions of the homogeneous fluid and the two-particle functions in the inhomogeneous case are functions of two or more variables, while the homogeneous two-particle functions only depend on the radial coordinate, and most of the inhomogeneous problems solved so far are those where the one-particle density is a function of

0953-8984/99/193789+10$19.50

one spatial variable. This increase in the number of variables usually implies a more complex theoretical approach and a numerical problem that is significantly more demanding [3, 4].

The earliest approximation for the three-particle distribution function of a homogeneous system was the superposition approximation of Kirkwood [5]. Subsequent improvements of this approximation [6–8] were based on some *ad hoc* correction functions determined from a general relation between $g^{(3)}$ and the isothermal pressure derivative of $g^{(2)}$ (see, e.g., [7, 8]). Other recent approaches [9, 10] made use of the integral equations formalism [11] and the inhomogeneous Ornstein–Zernike equation. This formalism was also used for the study of the two-particle structure of inhomogeneous fluids [12], for which density functional theories (DFT) have been also applied [3]. On the other hand, if one is interested in the triplet direct correlation function, it can be investigated via approximate factorization [8, 13] or even DFT [14].

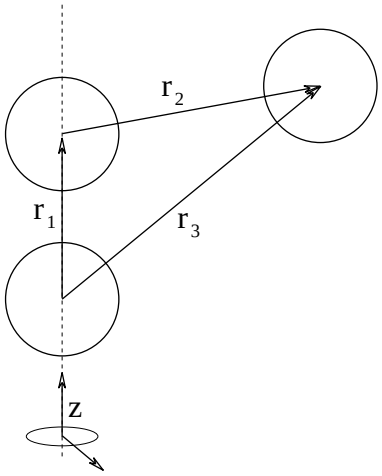

Figure 1. A schematic diagram of the problem. The dashed line shows the cylindrical axis of symmetry.

In this paper we shall focus on the calculation of the three-particle distribution function by means of the test-particle method. This procedure is based on an early idea of Percus for calculating the radial distribution function [15]: since $g(r)$ gives the probability of finding a particle of a fluid at a distance r from another particle, the inhomogeneous profile $\rho^{(1)}(\boldsymbol{r})$ of a fluid in contact with a particle fixed at the origin of coordinates is simply given by

$$\rho^{(1)}(\boldsymbol{r}) \equiv \rho^{(1)}(r) = \rho_{\mathrm{B}} g(r). \tag{2}$$

If *two* particles are fixed at a distance r_1, a similar probabilistic argument leads us to

$$\rho^{(1)}(\boldsymbol{r}) \equiv \rho^{(1)}(r_2, r_3) = \frac{\rho_{\mathrm{B}}}{g(r_1)} g^{(3)}(r_1, r_2, r_3) \tag{3}$$

and therefore

$$g^{(3)}(r_1, r_2, r_3) = \frac{g(r_1)}{\rho_{\mathrm{B}}} \rho^{(1)}(r_2, r_3). \tag{4}$$

A schematic representation of the problem is shown in figure 1. We note that this situation implies an external potential that depends on the positions of the two test particles and thus $\rho^{(1)}$ depends on the distances r_2 and r_3. Equation (4) is the key equation in our work, since it reduces the calculation of $g^{(3)}$ to the evaluation of the inhomogeneous profile $\rho^{(1)}$. Of course,

and as a first approximation, one can consider a superposition approximation (SA) scheme for $\rho^{(1)}$, i.e.,

$$\rho^{(1)}(r_2, r_3) \approx \rho_B g(r_2) g(r_3) \tag{5}$$

which when substituted into equation (4) leads to the usual Kirkwood superposition approximation (KSA) [5] for $g^{(3)}$:

$$g^{(3)}(r_1, r_2, r_3) \approx g(r_1) g(r_2) g(r_3). \tag{6}$$

In order to improve this KSA result, in this work we shall employ density functional theory to obtain the inhomogeneous profile $\rho^{(1)}(r_1, r_2)$.

In studying inhomogeneous fluids, density functional theories have become one of the most popular tools [16–18]. The accuracy of their predictions for a wide range of inhomogeneous problems is perhaps the main reason for their success. Of course, DFT also provides a theoretical framework for the study of homogeneous fluids. In this context it is important to mention here that the DFT framework allows ready calculation of the direct correlation functions (DCFs) $c^{(n)}$ via functional differentiation of the excess (over the ideal) free-energy functional w.r.t. the density $\rho^{(1)}(\boldsymbol{r})$ [17]. Thus, for $n = 2$ one can calculate the two-particle distribution function from $c^{(2)}$ and the Ornstein–Zernike relation (see, e.g., [17]). Using this procedure, Götzelmann *et al* [3] have recently obtained the two-particle distribution function for several problems of inhomogeneous hard-sphere fluids. For $n = 3$ one can also find a relation between $c^{(3)}$ and $g^{(3)}$ [8] but the calculation becomes very complicated. Thus, instead of following this approach, in this paper we shall consider the test-particle method of equation (4) where the profile $\rho^{(1)}(r_1, r_2)$ is obtained from DFT.

In DFT the profile is calculated by minimization of the grand potential of the fluid

$$\Omega[\rho] = \mathcal{F}[\rho] + \int \mathrm{d}\boldsymbol{r}\ \rho^{(1)}(\boldsymbol{r})[V_{\mathrm{ext}}(\boldsymbol{r}) - \mu] \tag{7}$$

where $\mathcal{F}[\rho]$ is the Helmholtz intrinsic free energy of the fluid and $V_{\mathrm{ext}}(\boldsymbol{r})$ is the external potential that gives rise to the inhomogeneity. In this case, the external potential is due to the interparticle potential of the two fixed particles. A DFT prescription provides an approximate form of the free energy $\mathcal{F}[\rho]$; in this work we have chosen the fundamental-measures theory of Rosenfeld [14] which appears to be one of the most successful theories for the study of hard-sphere fluids in very inhomogeneous situations [19].

In order to solve the equations arising in the minimization of $\Omega[\rho]$, we take advantage of the cylindrical symmetry of the system. This symmetry transforms a three-dimensional problem into a two-dimensional one, with coordinates z and ϱ for the symmetry and radial axis, respectively (see figure 1). For the numerical solution a two-dimensional grid is therefore employed. The calculations are done by means of Fourier transforms, more precisely fast Fourier transforms along the z-axis (this implies that we are assuming periodic boundary conditions along the symmetry axis) and Fourier–Bessel transforms (solved with the procedure described in [20]) along the ϱ-axis.

Either using the present test-particle DFT method or in the KSA scheme, the knowledge of the RDF $g(r)$ is needed. For the sake of consistency we have chosen to work with the $g(r)$ obtained by solving the original test-particle problem (equation (2)) with the same Rosenfeld DFT. Moreover, the ability of this DFT to describe $g(r)$ via the test-particle procedure can help us to explain its behaviour when employed to obtain $g^{(3)}$. In figure 2 we show a comparison between $g(r)$ obtained in a MC simulation (see below for details of the simulation) and the one obtained by solving the test-particle problem. Despite the high packing fraction $\eta_B = (1/6)\pi\sigma^3\rho_B = 0.4$ (the freezing occurs at a packing fraction $\eta_B \approx 0.47$), the DFT and simulation results are very close. The main differences arise near the first minimum, i.e., in

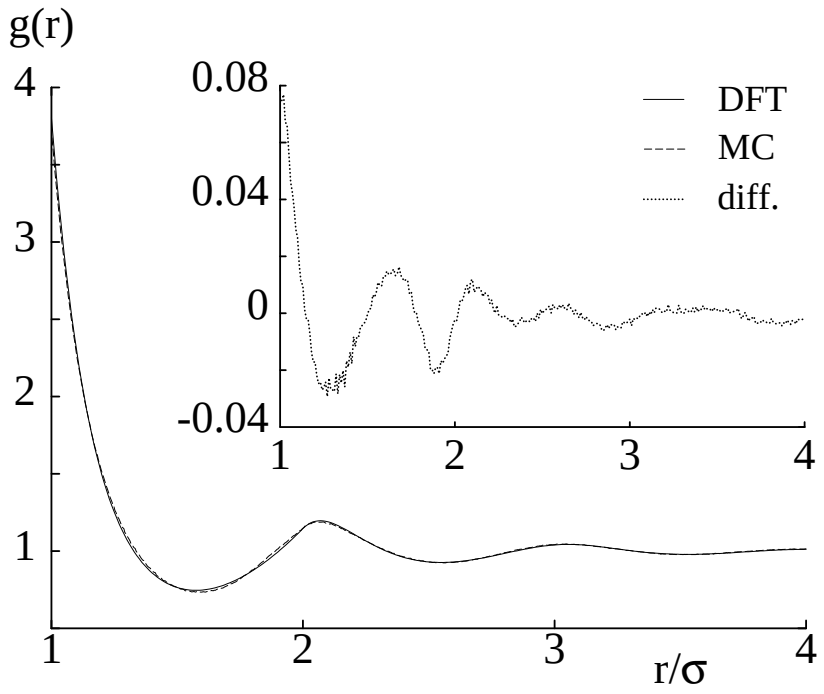

Figure 2. The RDF $g(r)$ of hard spheres calculated in the test-particle problem with DFT and MC simulation. The inset shows the difference between the two quantities. $\eta_B = 0.4$.

the zone around $r \approx 1.8\sigma$, and at contact ($r = \sigma^+$). These differences are very small and increase with density, as can be appreciated in table 1 where we present the values at contact $g(\sigma^+)$ obtained from DFT and simulation [21].

Table 1. Contact values $g(\sigma^+)$ obtained from DFT and simulation [21].

η	$g_{DFT}(\sigma^+)$	$g_{SIM}(\sigma^+)$
0.104758	1.312	1.312
0.209516	1.810	1.812
0.314075	2.644	2.635
0.340416	2.939	2.911
0.366557	3.280	3.239
0.392699	3.680	3.587
0.418841	4.153	4.031
0.444983	4.717	4.566
0.471315	5.403	5.185

The symmetry properties of $g^{(3)}$ can be exploited to obtain a consistency test of our procedure. More precisely, since

$$g^{(3)}(r_1, r_2, r_3) = g^{(3)}(r_2, r_3, r_1) = g^{(3)}(r_3, r_1, r_2) \tag{8}$$

from equation (4) we obtain

$$g(r_1)\rho^{(1)}(r_2, r_3) = g(r_2)\rho^{(1)}(r_3, r_1) = g(r_3)\rho^{(1)}(r_1, r_2) \tag{9}$$

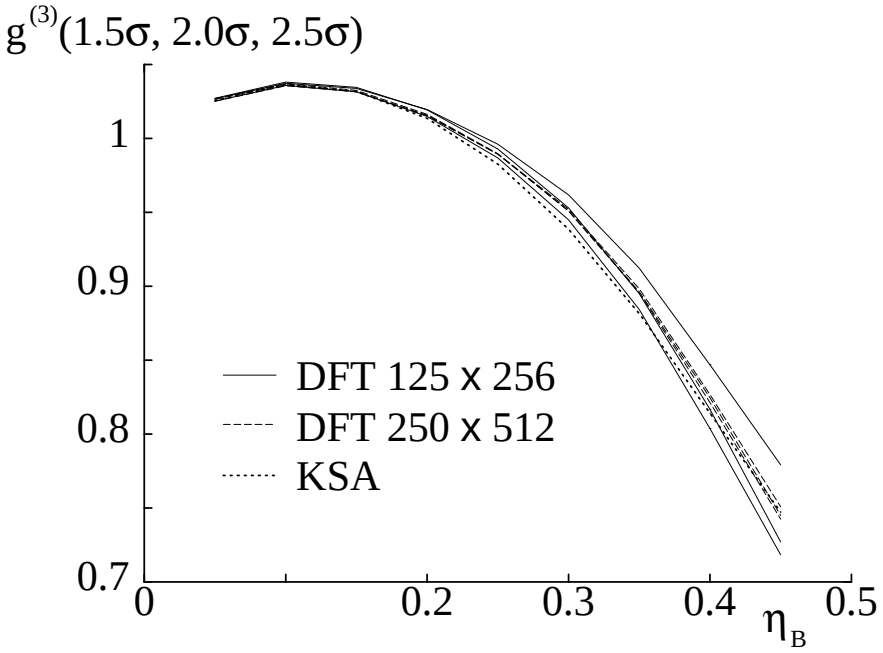

Figure 3. Comparison among the three-particle distribution functions $g^{(3)}(1.5\sigma, 2.0\sigma, 2.5\sigma)$ versus η_B obtained from the different choices of equation (9) (see the text), for two different grid sizes. The KSA result, using $g(r)$ from the test-particle DFT, is also shown.

where each profile is calculated for a given distance between the two fixed spheres. If the equalities in equation (9) are not fulfilled, this will be due to (a) the fact that we are not using the exact $g(r)$ but an approximate form and (b) the errors in the calculation of the profile ρ. These errors have, on the other hand, two origins: the approximate character of the DFT prescription and the approximations made in the numerical solution of the problem, the latter mainly due to the spacing of the mesh. We have observed that the choice of mesh is the most important source of errors, at least in the range of mesh spacings employed. In particular we have checked equation (9) for the case where $r_1 = 1.5\sigma$, $r_2 = 2.0\sigma$ and $r_3 = 2.5\sigma$. In figure 3 a plot of $g^{(3)}(1.5\sigma, 2.0\sigma, 2.5\sigma)$ for a wide range of densities and for two different meshes is shown. The three different lines for each mesh come from the three possibilities of equation (9). It is evident that the agreement between these three lines for the large grid (250×512 points) is much better than that for the small one (125×256 points). In the two cases we use 'boxes' of the same dimensions and large enough to ensure that the errors due to the finite size are not important. This dependence on the mesh spacing is not surprising since we are dealing with relatively small meshes, and trying to use them to 'simulate' circular curves (the test particles). Nevertheless, we consider the accuracy obtained with the large mesh reasonable, and in what follows we shall use it. In figure 3 we have also plotted the result obtained in the KSA (equation (6)), and found that in this case the results of DFT (large mesh) and from the KSA are comparable.

In order to compare with the DFT calculations, we have obtained the three-particle distribution function of the hard-sphere fluid from Monte Carlo simulation, but using two different methods. One method consists of performing a standard MC simulation of the homogeneous fluid where the value of $g^{(3)}$ is measured in a direct way by following the usual

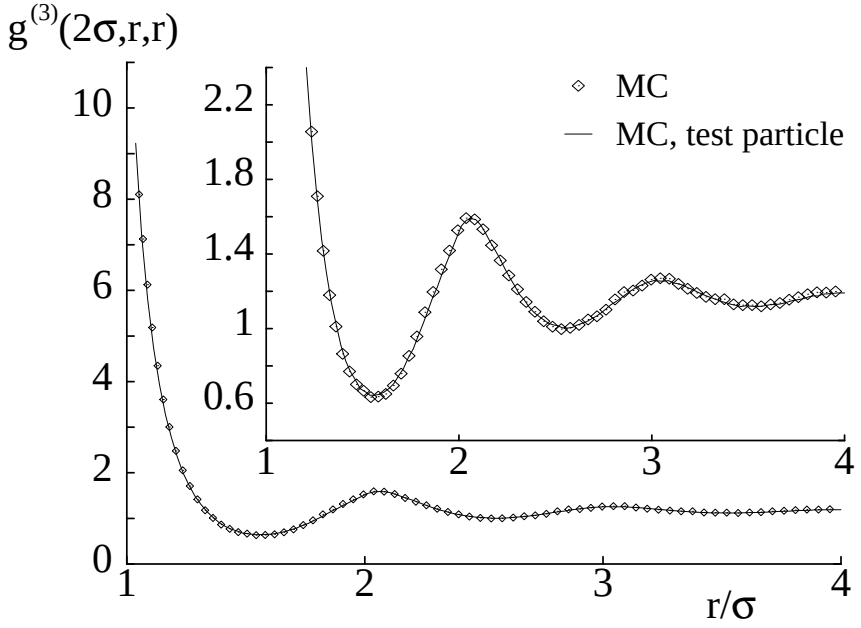

Figure 4. Comparison between the isosceles three-particle distribution functions $g^{(3)}(2\sigma, r, r)$ obtained from direct MC simulation and the test-particle method (equation (4)), where the inhomogeneous profile $\rho(2\sigma, r, r)$ has been obtained with a MC simulation (see the text). Bulk packing fraction $\eta_B = 0.4$. The inset shows a zoom on the vertical axis.

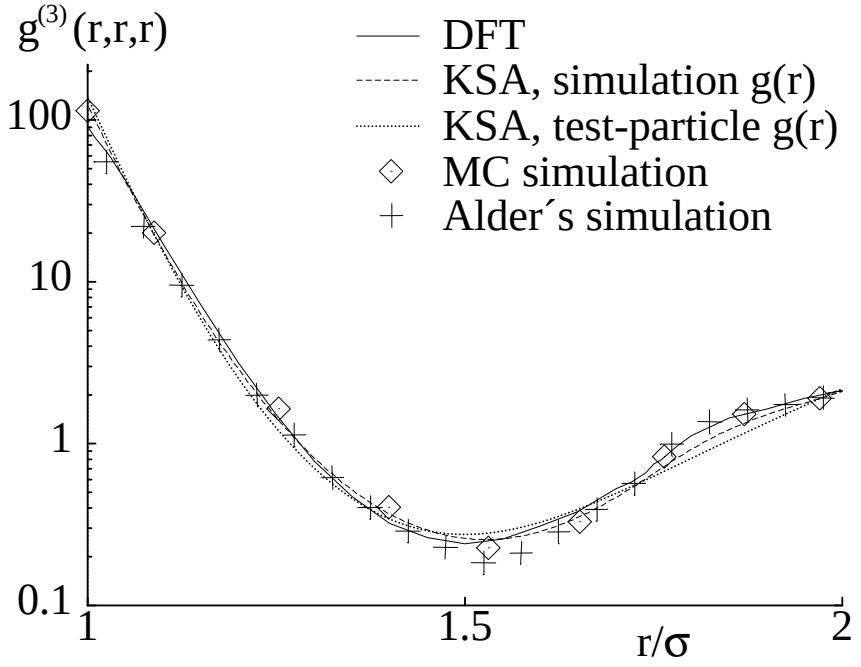

Figure 5. The three-particle distribution function $g^{(3)}(r, r, r)$ in the equilateral-triangle case. Bulk packing fraction $\eta_B = 0.463$. Notice the logarithmic scale on the vertical axis.

procedure (see, e.g., reference [4]). The other method is based on the test-particle argument of equation (4) and thus $g^{(3)}$ is calculated from the inhomogeneous profile obtained in a MC simulation of a fluid where two particles have fixed positions. The results from both methods are plotted in figure 4 where we observe that the only differences that arise are due to statistical errors in the simulations. This should be regarded as a test of the MC simulations. Both simulations were performed for a cubic 'box' of dimensions $12\sigma \times 12\sigma \times 12\sigma$ (σ being the hard-sphere diameter) and periodic boundary conditions, with $N = 1320$ spheres and 10^9 MC attempts per particle. This number of particles is large enough as to ensure that there are no effects due to the finite number of particles or boundary conditions. This is the scheme that we have followed in all of our MC simulations, and only the number of particles is changed to obtain data for different densities. It is worthwhile to mention that the long-range behaviour of $g^{(3)}$ is very sensitive to the structure of the fluid. Starting from a body-centred cubic grid of hard spheres, a very long thermalization run is needed ($\approx 10^7$ MC attempts per particle) in order to obtain a sensible result for the tail of $g^{(3)}$ (using the first method), while good results for $g(r)$ can be obtained with a much shorter thermalization ($\approx 10^4$ MC attempts).

As a case to study, in figure 5 we have focused on the case of equilateral symmetry ($r_1 = r_2 = r_3$) at a packing fraction $\eta_B = 0.463$. This case has already been studied by Alder [22] by means of molecular dynamics (MD) simulations, and as an additional test of our MC simulations we compare with their results, obtaining very good agreement. If we compare these simulation results with those obtained from our DFT procedure, we can see that the differences are very small and show the same trends in the region of the first

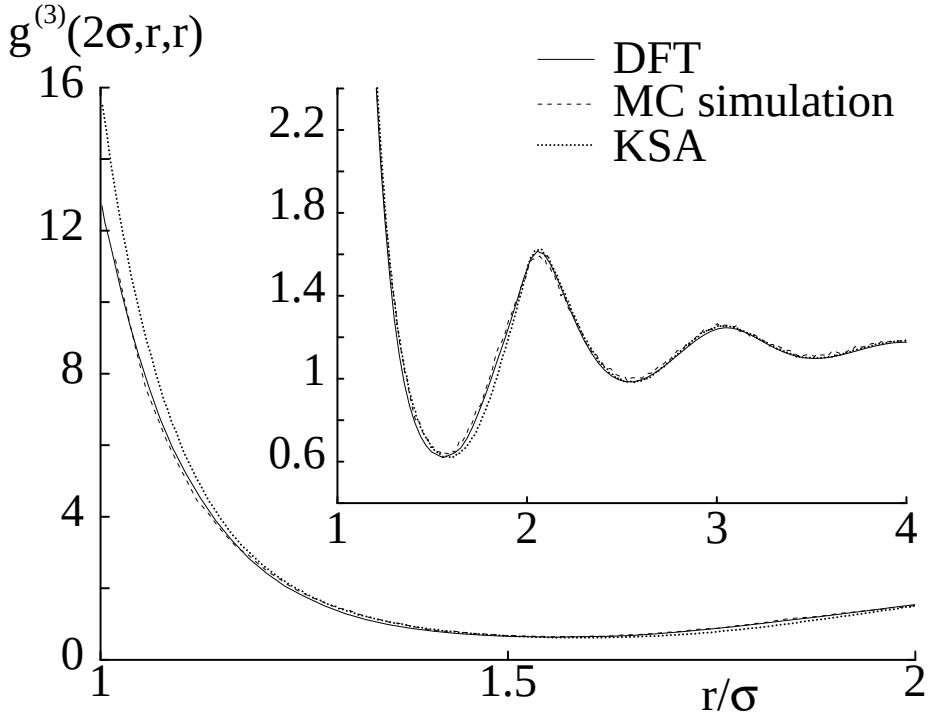

Figure 6. The isosceles three-particle distribution function $g^{(3)}(2\sigma, r, r)$. The absence of some results in the contact (small-r) region is due to the geometrical shape of the grid. Bulk packing fraction $\eta_B = 0.4$. The inset shows a zoom on the vertical axis.

minimum as previously observed in the $g(r)$ case (figure 2). One can infer that this behaviour is characteristic of Rosenfeld's DFT. On the other hand, the deviations of the DFT result near the contact, where a very inhomogeneous situation is reached—notice the very high value of $g^{(3)}$—can be ascribed to the approximate character of the theory but also to numerical problems related to the spacing of the grid. In figure 5 we also present KSA results (from MC simulation and DFT) and we observe that the KSA is unable to describe some of the features of $g^{(3)}$, especially in the region of $r \approx 1.8\sigma$. This behaviour is more evident when the $g(r)$ employed is obtained from the test-particle method, since this $g(r)$ is already an approximation.

Another possibility is to study the three-particle distribution function for isosceles (fixed r_1, and $r_2 = r_3$) configurations. If we consider the case where $r_1 = 2.0\sigma$ for $\eta_B = 0.4$, we find the situation depicted in figure 6. The main differences arise in the contact region, where DFT is clearly superior to the KSA (with $g(r)$ obtained from simulation). This contact reflects the situation where the three hard spheres are aligned and in contact with each other. In this case, it is reasonable for the superposition approximation to have some problems. On the other hand, if we look at the problem as an inhomogeneous fluid, this situation presents a very strong inhomogeneity, and the good behaviour of Rosenfeld's DFT is remarkable. Out of this region, the two results are very similar to simulation data. This is not very surprising if we look in figure 5 at the region near $r \approx 2.0\sigma$, where DFT and the KSA yield almost the same value. However, if we focus on the region near $r \approx 1.8\sigma$, where differences are bigger, we obtain the results depicted in figure 7. In this case, the behaviour of DFT is still very good and clearly superior to the KSA result, which presents important deviations from simulation at the first minimum.

Finally, the results for $g^{(3)}(2.0\sigma, r, r)$ obtained with the present approximation are

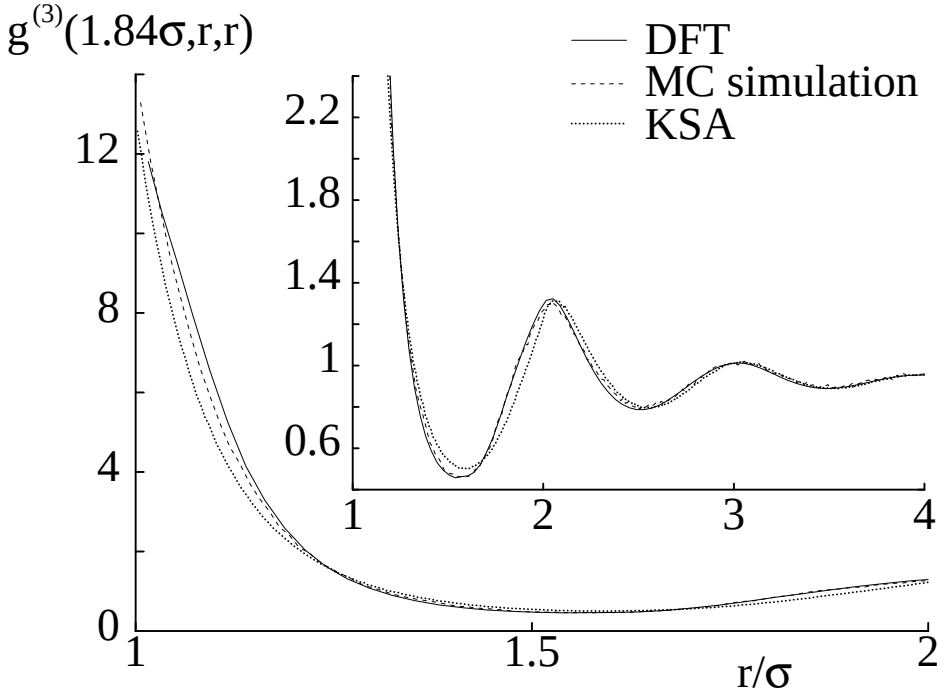

Figure 7. As figure 6, but for $g^{(3)}(1.84\sigma, r, r)$.

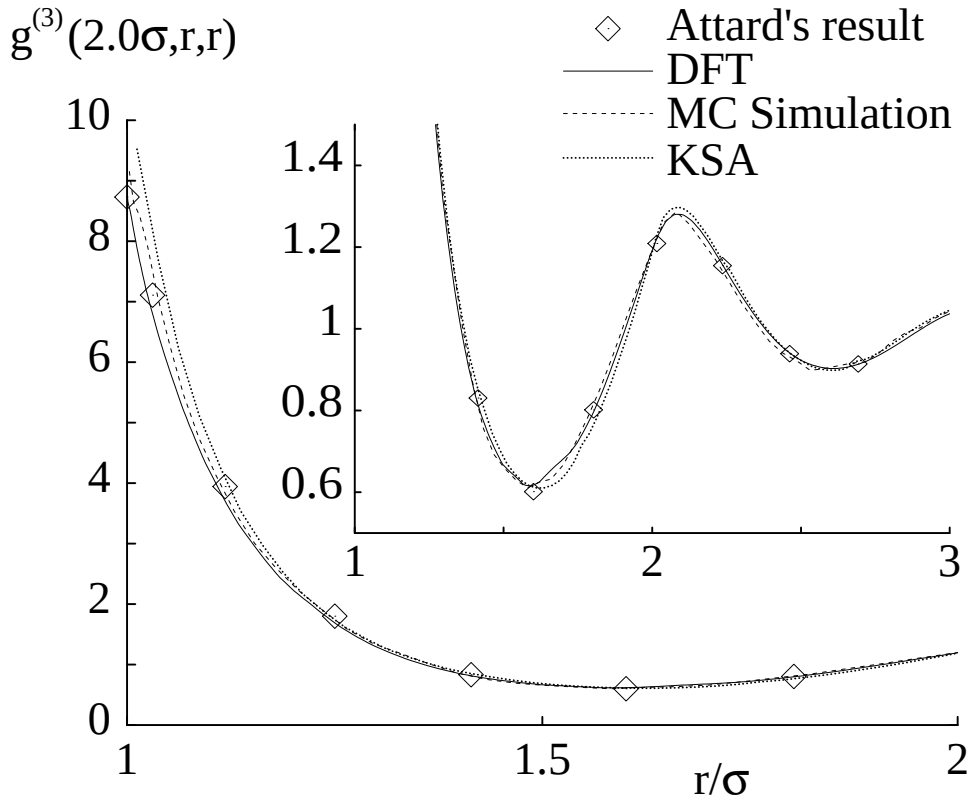

Figure 8. As figure 6, but for $\eta_B = 0.3666$.

compared with those obtained by Attard via the integral equations formalism [9]. We can see both results in figure 8, where simulation and KSA results are also shown. As one can observe, although Attard's theory seems to perform slightly better, the two theories yield comparable results. This fact is remarkable, since Attard's approximation employs a closure at the triplet level in the hierarchy of distribution functions [9].

To conclude, we shall summarize our results. We have presented in this work a different procedure for calculating the three-particle distribution functions of a hard-sphere fluid, using the test-particle and DFT methods. We have checked the dependency of the results on the numerics, and found that good results can be achieved with an adequate choice of the numerical parameters. When compared with simulations, the method is more accurate than the superposition approximation, and the small deviations that appear can be explained in terms of the approximate character of DFT.

Acknowledgments

The authors wish to acknowledge financial support by the Dirección General de Investigación Científica y Técnica (DGICYT) of Spain under Grant No PB 95-0934 and by Junta de Castilla y León (Spain) under Grant No SA78/96. AG is grateful for a fellowship from the Ministerio de Educación y Cultura of Spain.

References

[1] Hansen J-P and McDonald I R 1986 *Theory of Simple Liquids* (London: Academic)
[2] See, e.g., Henderson D (ed) 1992 *Inhomogeneous Fluids* (New York: Dekker)
[3] Götzelmann B, Haase A and Dietrich S 1996 *Phys. Rev.* E **53** 3456
Götzelmann B and Dietrich S 1997 *Phys. Rev.* E **55** 2993
[4] Hernando J A and Gamba Z 1992 *J. Chem. Phys.* **97** 5142
[5] Kirkwood J G 1935 *J. Chem. Phys.* **3** 300
[6] Egelstaff P A, Page D I and Heard C R T 1969 *Phys. Lett.* A **30** 376
[7] March N H 1990 *Chemical Physics of Liquids* (London: Gordon and Breach)
[8] Egelstaff P A 1992 *An Introduction to the Liquid State* 2nd edn (Oxford: Oxford University Press)
[9] Attard P 1989 *J. Chem. Phys.* **95** 3072
[10] Fushiki M 1991 *Mol. Phys.* **74** 307
Henderson D and Sokołowski S 1995 *J. Chem. Phys.* **103** 7541
Henderson D and Sokołowski S 1996 *J. Chem. Phys.* **104** 2974
[11] Henderson D 1992 *Inhomogeneous Fluids* ed D Henderson (New York: Dekker)
[12] Plischke M and Henderson D 1986 *Proc. R. Soc.* A **404** 323
[13] Barrat J-L, Hansen J-P and Pastore G 1987 *Phys. Rev. Lett.* **58** 2075
[14] Rosenfeld Y 1989 *Phys. Rev. Lett.* **63** 980
[15] Percus J K 1964 *The Equilibrium Theory of Classical Fluids* ed H L Frisch and J L Lebowitz (New York: Benjamin)
[16] Evans R 1979 *Adv. Phys.* **28** 143
[17] Evans R 1990 *Liquids at Interfaces (Les Houches Session 48)* ed J Charvolin, J F Joanny and J Zinn-Justin (Amsterdam: Elsevier)
[18] Evans R 1992 *Inhomogeneous Fluids* ed D Henderson (New York: Dekker)
[19] Rosenfeld Y 1993 *J. Chem. Phys.* **98** 8126 and references therein
[20] Lado F 1968 *J. Chem. Phys.* **49** 3092
[21] Groot R D, van der Eerden J P and Faber N M 1987 *J. Chem. Phys.* **87** 2263
[22] Alder B J 1964 *Phys. Rev. Lett.* **12** 317